Time-Resolved Resonance Raman Spectroscopic Studies on the Triplet Excited State of Thioxanthone

ARTICLE *in* THE JOURNAL OF PHYSICAL CHEMISTRY A · JUNE 2011

Impact Factor: 2.69 · DOI: 10.1021/jp202387v · Source: PubMed

2 AUTHORS:

Rishikesh Pandey
Massachusetts Institute of Technology
14 PUBLICATIONS **24** CITATIONS
SEE PROFILE

Siva Umapathy
Indian Institute of Science
143 PUBLICATIONS **1,432** CITATIONS
SEE PROFILE

THE JOURNAL OF PHYSICAL CHEMISTRY A

ARTICLE

pubs.acs.org/JPCA

Time-Resolved Resonance Raman Spectroscopic Studies on the Triplet Excited State of Thioxanthone

Rishikesh Pandey and Siva Umapathy*

Department of Inorganic and Physical Chemistry, Indian Institute of Science, Bangalore, India

Supporting Information

ABSTRACT: Thioxanthone has been investigated extensively owing to its unique photochemical and photophysical applications and its solvatochromic behavior. Here, we report the time-resolved resonance Raman studies on the structure of the lowest triplet excited state of thioxanthone in carbon tetrachloride. In addition, FT-IR and FT-Raman techniques have been used to study the vibrational structure in the ground state. To corroborate the experimental findings, density functional theory calculations have been carried out. Isotopic calculations and normal coordinate analysis have been used to help in assigning the observed bands to Raman vibrational modes. Structural information derived from this study is expected to help in better understanding the triplet state photochemistry of thioxanthone.

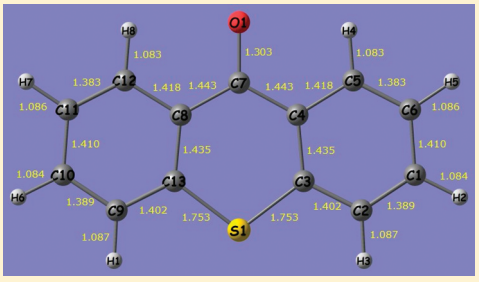

INTRODUCTION

The triplet states of aromatic ketones continue to receive attention from both the experimental and the theoretical points of view due to their role in various photochemical and photobiological reactions.[1−7] The molecule of interest in the present study, thioxanthone (TX), belongs to the aromatic ketone family and is well known for its cytotoxic activities. Further, TX and its derivatives have been demonstrated to have considerable antitumor properties and have great potential to be developed as novel antitumor agents.[8−11] TX and its derivatives are also efficient type-II photoinitiators in conjunction with tertiary amines under UV irradiation. Photoinitiation by this class of initiators is based on the reaction of the TX triplet excited state with a hydrogen donor, thereby producing an initiating radical.[12] Moreover, the thioxanthone derivatives also find extensive application in the dentistry resins and other curing and photopolymerization systems.[13]

Recently, the photoinduced electron-transfer reactions between the triplet excited state of TX with indolic and phenolic derivatives have been reported.[5,6,14] In most of the TX photochemistry, the long-lived lowest triplet state has been attributed to be responsible for the photosensitization reactions. It has also been shown that the photochemical reaction efficiency and relaxation behavior of carbonyl compounds can be correlated with the electronic state configuration ($\pi\pi^*$ or $n\pi^*$) of the lowest triplet excited state. In addition to the electronic nature of the excited triplet states, the structure/orientation also plays an important role that can be correlated to their reactivity.

The energy, lifetime, and the electronic configuration of the excited singlet and triplet states of TX have been studied by various spectroscopic techniques, including fluorescence, phosphorescence, and transient absorption spectroscopy.[15−22] It has attracted considerable attention of both the photophysicists and the photochemists due to its solvatochromic behavior.[15−20,22,23] The intensity and decay characteristics of the TX fluorescence strongly depend on the nature of the solvent. It has also been found that the triplet−triplet (T−T) absorption maximum is very sensitive to solvent polarity.[16,17] This dramatic solvent effect is attributable to the close-lying triplet excited states of two different configurations ($^3\pi\pi^*$ or $^3n\pi^*$), thus resulting in the substantial mixing of these states. Although the triplet state of TX has been extensively studied, the vibrational structure of TX in the triplet state has not been reported.

This paper deals with the vibrational structural characterization of both ground and triplet states of TX using both experimental and computational methods. To the best of our knowledge, the detailed vibrational analysis of TX in the ground state as well in the triplet excited state has not been reported. For the ground-state experimental study, FT-Raman and FT-IR techniques have been employed, whereas the time-resolved resonance Raman technique (TR^3) has been used for the triplet state study. TR^3 is known to be an excellent technique for probing the structure of the transient species formed during the course of photochemical/photophysical reactions.[24−28] In this paper, the excited triplet state structure of TX in carbon tetrachloride (CCl_4) has been investigated. The results of the DFT calculations have also been used to understand the molecular structure details in the triplet state. We would like to note that we have chosen CCl_4 because it is known to be an noninteracting solvent and, further, CCl_4 has a much fewer number of interfering solvent Raman bands. A similar study on this molecule in solvents of differing polarities is underway.

Received: March 14, 2011
Revised: May 25, 2011
Published: May 25, 2011

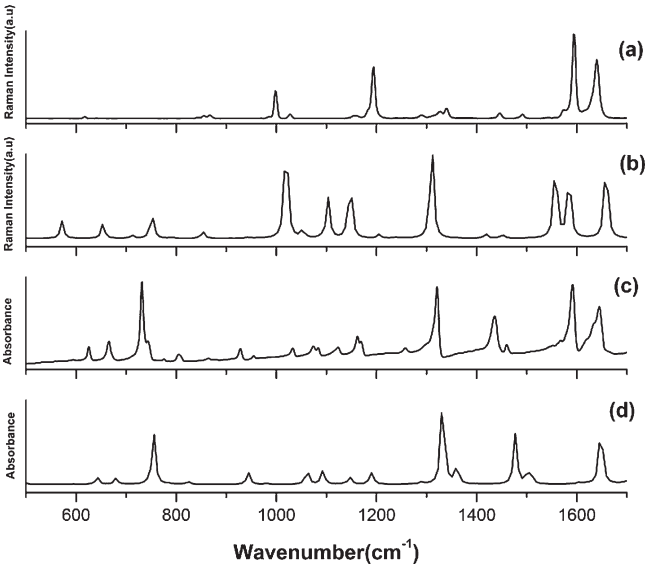

Figure 1. FT-Raman (a), computed Raman (b), FT-IR (c), and computed IR spectra (d) of the ground state of TX.

EXPERIMENTAL SECTION

The detailed experimental setup and the procedures used for TR^3 spectroscopy have been described previously.[25] Briefly, the third harmonic 355 nm laser pulse (pulse width, 8−10 ns; 10 Hz; 3 mJ) from a Nd:YAG laser (DCR 11, Spectra Physics) was used as the photoexcitation (pump) source. The 634 nm probe pulse (pulse width, 8−10 ns; 10 Hz; 2 mJ) was generated by a home-made hydrogen Raman shifter that was pumped by another Nd:YAG laser (GCR 250, Spectra Physics) providing a high-energy laser pulse with a wavelength of 355 nm. A SPEX 1404 double monochromator was used with two 600 groove gratings to disperse the scattered light. A liquid-N_2-cooled CCD (Jobin Yvon) with 1024 × 256 pixels was used as the multichannel detector. The recorded Raman spectra were calibrated using known solvent bands as a reference, and the spectral resolution was estimated as 5 cm^{-1}. The sample solutions (~2.5 mM) were circulated through a capillary at a rate of ca. 20 mL/min such that each sample volume received only one laser pulse of the 10 Hz laser system. To avoid possible accumulation of photoproducts, the sample solution was replaced regularly with the fresh solution. In addition, the ground-state Raman spectrum was also recorded at various times and recorded spectra were compared with the initially recorded (at the start of the experiment) ground-state spectrum, and it was noted that the accumulation of photoproducts was not present or negligibly small. The transient absorption measurement was carried out using an Applied Photophysics LKS.60 spectrometer. The 355 nm photoexcitation laser pulse was obtained from the third harmonic of a Nd:YAG laser (DCR 11, Spectra Physics). The probe light source was from a 250 W pulsed xenon lamp, and signals were detected using a Czerny Turner monochromator and an R-928 five-stage photomultiplier tube. The transient signals were acquired and analyzed with a combination of an oscilloscope and a personal computer, and a sample cell with a 1 cm path length was used in the present study.

TX, purchased from Aldrich, was of high-purity grade (97%) and vacuum-sublimed before use. The spectroscopic grade CCl_4 was also purchased from Aldrich and used as received. The FT-IR spectrum of TX was recorded at room temperature on a Bruker Optics Alpha-P FT-IR spectrometer by making KBr pellets. The FT-Raman spectrum was recorded in solid phase on a Bruker Optics MultiRAM FT-Raman spectrometer at a 4 cm^{-1} resolution.

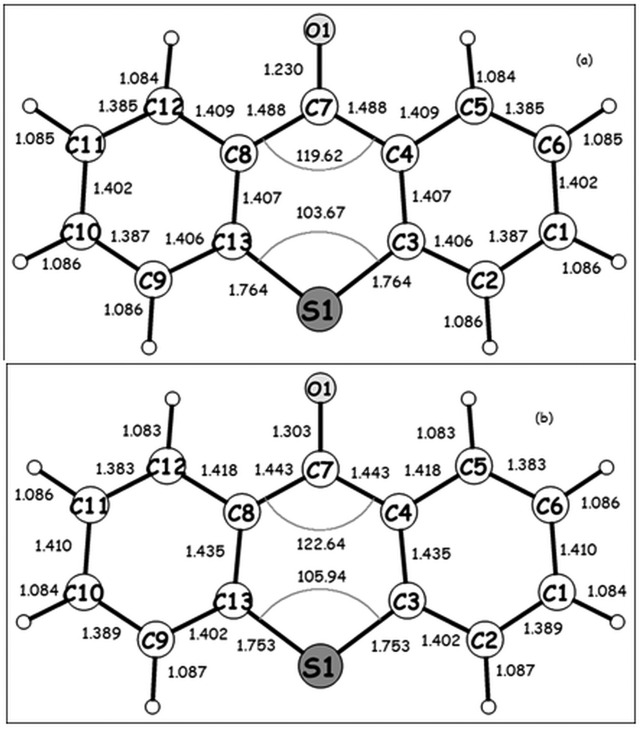

Figure 2. Optimized geometry of the TX ground state (a) and triplet excited state (b).

COMPUTATIONAL DETAILS

The quantum-mechanical calculations of the structure and frequencies of the normal vibrations in the singlet and triplet states (S_0 and T_1) were performed by the DFT/B3LYP/6-31G(d,p) method as implemented in Gaussian 03.[29] The basis set 6-31G(d,p) was chosen as it is known to reproduce experimental frequencies accurately on structurally similar systems.[6,30−32] The full geometry optimization was carried out using Berny's optimization algorithm. The complete geometry optimization was done with two types of initial geometry, one with no symmetry and other with an initial C_{2v} symmetry (planar). To include the solvent effect, the polarizable continuum model (PCM) has been employed in the frequency calculation.[29,33] The vibrational frequencies and the corresponding normal modes were evaluated for the optimized geometries using an analytical differentiation algorithm contained within the program. The optimized structure of TX in both the ground state as well as the excited state were confirmed to be stationary points as the frequency calculation did not find any imaginary frequency. Computed vibrational frequencies were scaled in order to have better correspondence with experimental results. We have used a scaling factor value of 0.9614, which has been used previously.[34] The optimized structure and the calculated normal modes of vibration were visualized using Chemcraft software (http://www.chemcraftprog.com), and the VEDA 4.0 program (vibrational energy distribution analysis) was used for the potential energy distribution calculations.[35] Additional structural analysis of the bonding properties has been carried out using the NBO (natural bond order) method as included in the Gaussian 03 program suite.[36]

RESULTS AND DISCUSSION

Before discussing the structure of TX in the triplet excited state, it is important to understand the structure of the molecule in the ground state. FT-Raman and FT-IR spectra of TX in the ground state are presented in Figure 1a,c, respectively, along with the DFT calculated Raman (Figure 1b) and IR spectra (Figure 1d).

Geometrical Structure. *Ground State.* The geometrical structure of TX was optimized using the DFT/B3LYP/6-31G(d,p) method. The full geometry optimization was first carried out with an initial C_{2v} symmetry, resulting in an optimized planar structure with the same symmetry. The optimized structure of TX in the ground state along with the atom numbering is presented in Figure 2a. The DFT calculated optimized parameters along with the experimental parameters are presented in Table 1. As can be seen from Table 1, the calculated average parameters in the present study are comparable to the gas-phase electron diffraction results,[37] except the dihedral angle, which is 180° and differs from the experimentally reported value of 173.3°. This signifies that benzene rings are bent and TX is nonplanar. Further, the earlier calorimetry study[38] also substantiates the slight nonplanarity in the TX structure.

To understand the differences in the calculated value of the dihedral angle from the reported experimental data, the full geometry optimization was also carried out with an initial nonlanar geometry. Although the full geometry optimization of TX from an initial nonplanar geometry gives a slightly nonplanar structure with C_s symmetry, the optimized parameters (bond lengths and bond angles) are not significantly different from the planar optimized geometry (obtained from an initial C_{2v} symmetry). The zero-point-corrected energies of both the conformers have been calculated and found to be similar. MP2 level calculation on the S_0 of TX has also been reported, indicating that the energy difference between the planar and nonplanar conformations is very small.[39] It is notable that the results obtained from both DFT and MP2 methods are very similar except for the dihedral angle and out-of-plane angle (Table 1). Because there was no significant difference between the bond lengths and bond angles of the two conformers (Table 1), we have chosen the planar geometry for the frequency calculation.

Triplet Excited State. The optimized geometry of TX in the lowest triplet state (T_1) is presented in Figure 2b. The optimized ground-state geometry was taken as the initial geometry for the triplet state optimization leading to the planar geometry. It is interesting to compare the main structural parameters, which

Table 1. Main Structural Parameters for the Ground State and Lowest Triplet State of TX: Method, DFT; Functional, B3LYP; Basis Set, 6-31G(d,p)[a,b]

	ground state (calcd)[c]			
parameter	planar C_{2v}	nonplanar C_s	ground state (exptl)[e]	triplet state (calcd)
r_{C1-C2}	1.387 (1.386)	1.387 (1.386)	1.401[d]	1.389
r_{C2-C3}	1.406 (1.407)	1.406 (1.407)	1.401[d]	1.402
r_{C3-C4}	1.407 (1.406)	1.407 (1.406)	1.401[d]	1.435
r_{C4-C5}	1.409 (1.408)	1.409 (1.408)	1.401[d]	1.418
r_{C5-C6}	1.385 (1.386)	1.385 (1.386)	1.401[d]	1.383
r_{C6-C1}	1.402 (1.403)	1.402 (1.403)	1.401[d]	1.410
r_{C-H}	1.085[d](1.087)	1.083[d](1.087)	1.087[d]	1.085[d]
r_{C4-C7}	1.488(1.483)	1.487	1.498	1.443
r_{C7-O}	1.230 (1.239)	1.230 (1.239)	1.232	1.303
r_{C3-S}	1.764 (1.754)	1.764 (1.754)	1.751	1.753
$\varphi_{C3-S-C13}$	103.7 (103.3)	103.7 (103.1)	103.4	105.9
$\delta_{C4-C3-S-C13}$	180.0 (0.0)	179.99 (173.3)	169.0	0.0
$\delta_{C5-C4-C7-O}$	0.0 (0.0)	0.0 (4.1)		0.0
$\varphi_{C8-C7-C4}$	199.6			122.6

[a] For numbering, see Figure 2. [b] All bond lengths are given in Å, all angles in degrees. [c] The values given in parentheses are from ref 39. [d] Averaged value. [e] Electron diffraction measurement, ref 37.

Table 2. Natural Charges and "Totals by Atom"' Wiberg Bond Indices of TX and Xanthone

	thioxanthone				xanthone			
	ground state		triplet state		ground state		triplet state	
atom	charge[a]	B.I.[b]	charge[a]	B.I.[b]	charge[a]	B.I.[b]	charge[a]	B.I.[b]
C1	−0.10270	3.9435	−0.25436	3.8425	−0.20584	3.9436	−0.23418	3.8566
C2	−0.12422	3.9423	−0.24192	3.9108	−0.27506	3.9402	−0.27996	3.9213
C3	−0.08784	3.9998	−0.21464	3.8846	0.34489	3.8927	0.33794	3.8345
C4	−0.07697	3.9947	−0.05553	3.9019	−0.19283	3.9881	−0.15133	3.9426
C5	−0.08652	3.9289	−0.23177	3.8716	−0.17405	3.9312	−0.22846	3.8452
C6	−0.12323	3.9432	−0.19119	3.8892	−0.25463	3.9427	−0.24383	3.9362
C7	0.26747	3.9125	0.27992	3.7470	0.52953	3.9188	0.27152	3.5814
C8	−0.07697	3.9947	−0.05553	3.9019	−0.19283	3.9881	−0.15133	3.9426
C9	−0.12422	3.9423	−0.24192	3.9108	−0.27506	3.9402	−0.27996	3.9213
C10	−0.10270	3.9435	−0.25436	3.8425	−0.20584	3.9436	−0.23418	3.8566
C11	−0.12323	3.9432	−0.19119	3.8892	−0.25463	3.9427	−0.24383	3.9362
C12	−0.08652	3.9289	−0.23177	3.8716	−0.17405	3.9312	−0.22846	3.8452
C13	−0.08784	3.9998	−0.21464	3.8846	0.34489	3.8927	0.33794	3.8345
O1	−0.28651	2.0125	−0.49976	1.4904	−0.57017	2.0163	−0.17487	1.2666
S1(O2)[c]	0.21281	2.5014	0.58245	2.4363	−0.47058	2.2339	−0.47915	2.1711

[a] Natural charge obtained from NBO analysis. [b] "Totals by atom" Wiberg bond index. [c] S1 is replaced by O2 in the case of xanthone. Atom labeling is given in Fig 2.

Table 3. Ground-State Experimental (Raman and IR) and Calculated Frequencies and Their Assignments[a,b]

mode	S	freq (calcd)[c]	FTR (exptl)	FT-IR (exptl)	% PED	approx character
ν_{16}	A_1	572		594	$^{\delta}$C13C8C7 19, $^{\delta}$C2C1C6 −11, $^{\delta}$C11C10C9 −11	ring def (central ring)
ν_{17}	B_2	618		625	$^{\delta}$OC7C8 13, $^{\delta}$C10C9C13 −20, $^{\delta}$C3C2C1 16	ring def (outer ring)
ν_{18}	B_1	653	618		$^{\tau}$C5C6C1C2 13, $^{\tau}$C12C11C10C9 −12, $^{\tau}$OC4C8C7 −22	CCCC torsion
ν_{19}	A_1	654	640	666	$^{\delta}$C12C11C10 15	CCC bend
ν_{21}	B_2	712		744	$^{\nu}$SC 19, $^{\delta}$C5C6C1 21, $^{\delta}$C12C11C10 −11, $^{\delta}$OC7C8 11	CCC bend
ν_{22}	B_1	726		731	$^{\tau}$H2C1C6C5 −10, $^{\tau}$H5C6C5C4 −10, $^{\tau}$H6C10C11C12 10, $^{\tau}$H7C11C12C8 10	oop C−H wag (sym)
ν_{23}	A_2	747		757	$^{\tau}$H2C1C6C5 14, $^{\tau}$H3C2C3C4 −11, $^{\tau}$H5C6C5C4 18, $^{\tau}$H1C9C13C8 −11, $^{\tau}$H6C10C11C12 14, $^{\tau}$H7C11C12C8 18	oop C−H wag (asym)
ν_{24}	A_1	754		776	$^{\delta}$C2C1C6 12, $^{\delta}$C11C10C9 11, $^{\delta}$C8C7C4 −16	CCC bend
ν_{25}	B_1	792	843	805	$^{\tau}$H3C2C3C4 10, $^{\tau}$H1C9C13C8 −10,$^{\tau}$OC4C8C7 36, $^{\tau}$C7C3C5C4 10	torsion OCCC
ν_{26}	A_2	850	856	864	$^{\tau}$H3C2C3C4 21, $^{\tau}$H4C5C6C1 −10, $^{\tau}$H5C6C5C4 16, $^{\tau}$H1C9C13C8 21, $^{\tau}$H7C11C12C8 16, $^{\tau}$H8C12C11C10 −10	oop C−H bend
ν_{27}	B_1	853	867	877	$^{\tau}$H3C2C3C4 16, $^{\tau}$H5C6C5C4 18, $^{\tau}$H1C9C13C8 −16, $^{\tau}$H7C11C12C8 −18	oop C−H bend
ν_{28}	B_2	908		928	$^{\delta}$OC7C8 −13, $^{\delta}$C2C1C6 −14, $^{\delta}$C10C9C13 −10, $^{\delta}$C11C10C9 14, $^{\delta}$C9C13C8 10	CCC bend
ν_{30}	B_1	943	916		$^{\tau}$H2C1C6C5 −24, $^{\tau}$H3C2C3C4 −11, $^{\tau}$H4C5C6C1 −11, $^{\tau}$H1C9C13C8 11, $^{\tau}$H6C10C11C12 24, $^{\tau}$H8C12C11C10 11	torsion HCCC
ν_{31}	A_2	969		955	$^{\tau}$H4C5C6C1 16, $^{\tau}$H5C6C5C4 13, $^{\tau}$H7C11C12C8 13, $^{\tau}$H8C12C11C10 16, $^{\tau}$C5C6C1C2 11, $^{\tau}$C12C11C10C9 12	oop C−H bend
ν_{32}	B_1	970	985		$^{\tau}$H4C5C6C1 −18, $^{\tau}$H5C6C5C4 −13, $^{\tau}$H7C11C12C8 13, $^{\tau}$H8C12C11C10 18, $^{\tau}$C5C6C1C2 −10, $^{\tau}$C12C11C10C9 12	torsion HCCC
ν_{33}	A_1	1019	998	999	$^{\nu}$C1C6 25, $^{\nu}$C11C10 22	sym ring breath
ν_{34}	B_2	1021	1027	1033	$^{\nu}$C1C6 −14, $^{\nu}$C11C10 23	asym ring breath
ν_{35}	B_2	1050		1074	$^{\delta}$C12C11C10 −11, $^{\delta}$C10C9C13 −12, $^{\delta}$C4C3C2 14	CCC bend
ν_{36}	A_1	1052	1059	1084	$^{\delta}$C5C6C1 −13, $^{\delta}$C12C11C10 −13, $^{\delta}$SC3C2 −10	CCC bend
ν_{37}	B_2	1094		1123	$^{\nu}$C3C2 12	CC str
ν_{38}	A_1	1104	1156	1169	$^{\nu}$C9C13 12, $^{\delta}$H4C5C6 12, $^{\delta}$H8C12C11 −12	CCH bend
ν_{39}	A_1	1143		1162	$^{\delta}$H2C1C2 −18, $^{\delta}$H3C2C3 10, $^{\delta}$H1C9C1310, $^{\delta}$H6C10C11 14	CCH bend
ν_{41}	A_1	1149	1195		$^{\delta}$H5C6C1 −20, $^{\delta}$H7C11C12 21	sci CCH
ν_{42}	B_2	1205		1222	$^{\nu}$C3C2 11, $^{\nu}$C9C13 −12, $^{\delta}$H3C2C3 16, $^{\delta}$H1C9C13 16	CCH bend
ν_{43}	A_1	1241	1290	1257	$^{\delta}$H3C2C316, $^{\delta}$H4C5C6 16, $^{\delta}$H1C9C13 16, $^{\delta}$H8C12C11 16	CCH
ν_{44}	B_2	1281		1320	$^{\nu}$C7C4 −20, $^{\nu}$C8C7 17	CC str
ν_{45}	B_2	1306	1327		$^{\nu}$C12C11 12, $^{\nu}$C4C3 −17, $^{\nu}$C13C8 20	CC str
ν_{46}	A_1	1310	1340		$^{\nu}$C5C6 14, $^{\nu}$C12C11 13, $^{\nu}$C3C2 10, $^{\nu}$C13C8 18	CC str
ν_{47}	A_1	1418	1446		$^{\delta}$H2C1C2 −14, $^{\delta}$H5C6C1 −15, $^{\delta}$H6C10C11 14, $^{\delta}$H7C11C12 14	CCH bend
ν_{48}	B_2	1420		1436	$^{\delta}$H2C1C2 14, $^{\delta}$H5C6C1 11, $^{\delta}$H6C10C11 14, $^{\delta}$H7C11C12 10	CCH bend
ν_{49}	B_2	1444		1460	$^{\delta}$H3C2C3 −13, $^{\delta}$H4C5C6 11, $^{\delta}$H1C9C13 13, $^{\delta}$H8C12C11 −11	CCH bend
ν_{50}	A_1	1451	1492	1509	$^{\delta}$H3C2C3 −14, $^{\delta}$H4C5C6 10, $^{\delta}$H1C9C13 −14, $^{\delta}$H8C12C11 10	CCH bend
ν_{51}	B_2	1543	1543	1551	$^{\nu}$C1C6 −10, $^{\nu}$C13C8 12	CC str
ν_{52}	A_1	1557	1574	1567	$^{\nu}$C2C1 10, $^{\nu}$C10C9 10, $^{\nu}$C13C8 −14	CC str
ν_{53}	B_2	1584	1595	1592	$^{\nu}$C2C1 −14, $^{\nu}$C5C614, $^{\nu}$C10C9 14, $^{\nu}$C11C12−16	CC str
ν_{55}	A_1	1659	1640	1645	$^{\nu}$CO 83	CO str

[a] Abbreviations: S, symmetry; ν, stretching; δ, bending; τ, torsion; oop, out-of-plane; def, deformation. [b] All frequencies in cm^{-1}. [c] Calculated with DFT B3LYP/6-31G(d,p); uniform scaling factor = 0.9614.

significantly change while going from ground state to triplet state. It is observed from Table 1 that there is a considerable increase in the C═O bond length in the triplet excited state as compared with the ground state (from 1.23 to 1.30 Å) and it acquires a partial single bond character. The bonds connected to C7 (carbon connected to the oxygen atom) are short in the triplet state (from 1.49 to 1.44 Å), which signifies an increase in the electron density on the carbon−oxygen bond as compared with the ground state. In addition, there is an increase in the C4−C3 (or C8−C13) bond lengths (from 1.41 to 1.44 Å) along with an increase in the C8−C7−C4 angle (119.6−122.6°) when we go from the ground state to the triplet excited state. A similar increase has also been noticed for the C13−S−C3 angle (103.7−105.9°), signifying that the central ring gets distorted upon excitation.

dx.doi.org/10.1021/jp202387v |J. Phys. Chem. A 2011, 115, 7566–7573

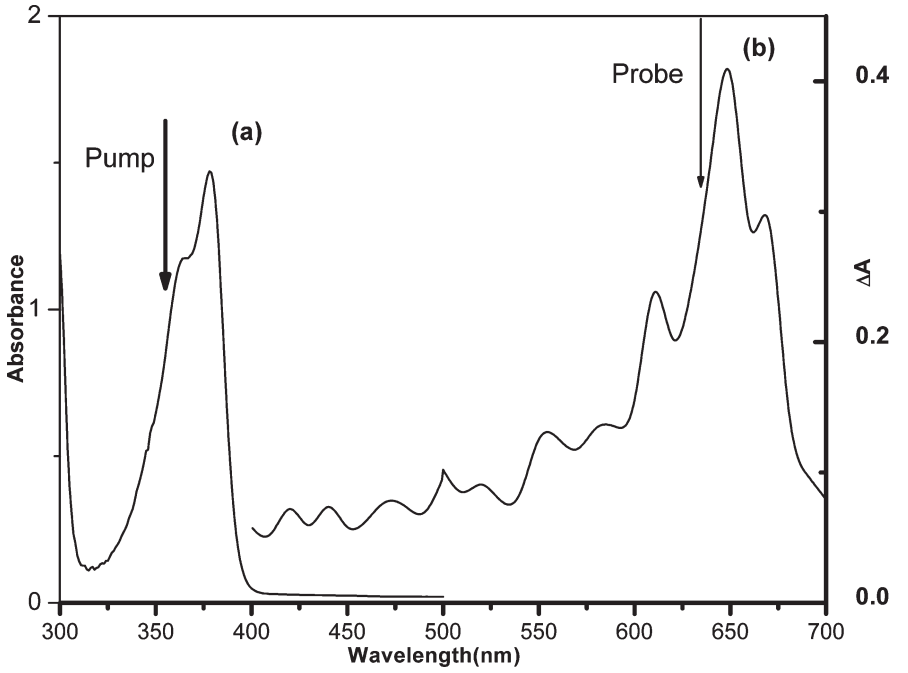

Figure 3. Absorption spectrum of S_0 (a) and T_1 (b) states of TX. The arrows show the pump and probe wavelengths, respectively, chosen in the present study.

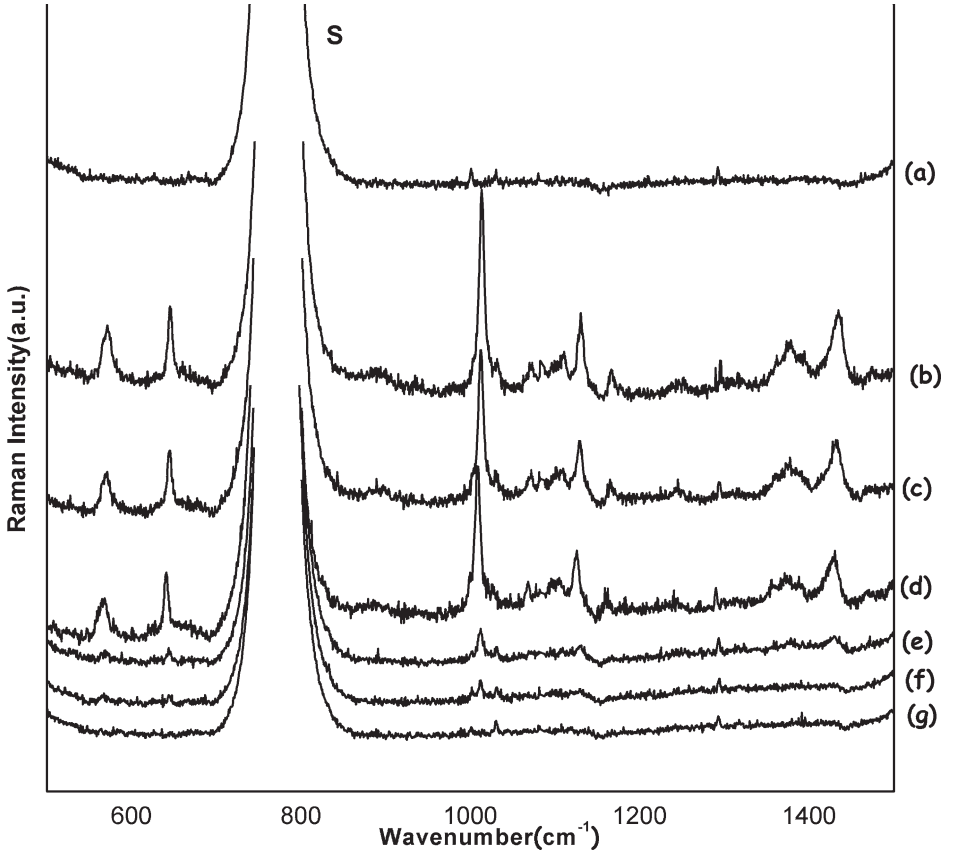

Figure 4. Time-resolved resonance Raman spectra of TX (~2.5 mM) in CCl_4 at various delay times (pump laser at 355 nm, probe laser at 634 nm): (a) −50 ns, (b) 50 ns, (c) 100 ns, (d) 200 ns, (e) 400 ns, (f) 600 ns, (g) 800 ns. Pump-only and probe-only spectra were subtracted from the pump + probe spectra.

NBO Analysis. To give further insights into the structural analysis and also to understand the role of the sulfur atom in TX, natural bond order analysis has been carried out on the optimized geometries of both thioxanthone and xanthone (a structurally similar molecule where sulfur has been replaced with the oxygen atom) for the ground and the lowest triplet states. The natural charges on the heavy atoms along with the "totals by atom" Wiberg indices[40] of thioxanthone and xanthone for their ground as well as triplet states are presented in Table 2. As can been seen from the table, the "totals by atom" Wiberg bond index for the carbonyl carbon (C7) and carbonyl oxygen (O1) for both the molecules in their ground states are very similar, which is consistent with the calculated similar C−O bond order of 1.69 and 1.70 for thioxanthone and xanthone, respectively. In the case of the triplet state, total Wiberg bond indices of the carbonyl carbon and oxygen for both the molecules are significantly different (refer to Table 2) and the C−O bond order of the carbonyl bond is 1.28 and 1.15 for thioxanthone and xanthone triplet state, respectively. It can be seen from Table 2 that, in the case of the triplet state of TX, electron redistribution takes place to a greater extent than the triplet of the xanthone. Further, the triplet excitation seems to affect the electron clouds of both the heteroatoms of TX, whereas in the case of xanthone, only one of the heteroatoms, that is, the carbonyl oxygen, is significantly affected. It is, therefore, expected that the triplet state reactivity of TX should be different than that of the xanthone counterpart. The dipole moments of TX in the ground and lowest triplet excited states have been calculated to be 2.40 and 3.62 D, respectively, which implies that the triplet state is more polar than the ground state.

Vibrational Assignments of the Ground State. TX is composed of 23 atoms; hence, it has 63 normal modes. Having assumed that TX belongs to the C_{2v} symmetry, its vibrations are distributed among the symmetry species as follows: $22A_1 + 9A_2 + 11B_1 + 21B_2$. The symmetries and frequencies of the DFT calculated normal modes, experimental IR and Raman frequencies, approximate description of the calculated normal modes, along with the PEDs, are presented in Table 3. Since excitation wavelength (1064 nm) used in the FT-Raman measurement is not in resonance with any of the electronic transitions of TX, the calculated non resonant Raman activities (intensities) of the normal modes have been used to assign the bands. In addition, the isotopic frequency calculations on four isotopomers of TX, $C_{13}H_8O^{18}S$, $C_{13}H_8OS^{34}$, $C_{12}{}^7C^{14}H_8OS$ (C^{14} isotope and carbon at seventh position in Figure 2), and $C_{12}{}^3C^{14}H_8OS$, have also been carried out, and the calculated frequencies are listed in Table S1 (Supporting Information).

First, we focus our discussion on the band assignments of some of the important and intense bands observed in either the IR or the Raman spectrum. Detailed assignments of all the experimentally observed bands are presented in Table 3. The FT-Raman spectrum of TX shows two intense bands at 1640 and 1595 cm^{-1} corresponding to two intense IR bands at 1645 and 1592 cm^{-1} in the 1500−1700 cm^{-1} range. We correlate these two experimentally observed bands to the calculated frequencies of 1659 and 1584 cm^{-1}. The 1640 cm^{-1} Raman band and the corresponding 1645 cm^{-1} IR band can both be assigned to the C═O stretch. This assignment can further be supported by shifts in the computed frequencies upon isotopic substitution in the C═O group (the 1659 cm^{-1} band shifts to 1630 and 1601 cm^{-1} upon O^{18} and C^{14} substitutions, respectively) . As can be seen in Table 3, this band has a contribution mostly (83%) from the C═O stretching mode. The intense band at 1595 cm^{-1} in the Raman spectrum and 1592 cm^{-1} band in the IR spectrum can be assigned to the C═C fundamental of the ring and can be correlated with the calculated normal mode frequency at 1584 cm^{-1}. Further, this is supported by the isotopic calculation on TX by substituting (C^{12} to C^{14}) to the carbon atoms that are connected to the oxygen and sulfur atoms (Table S1). The intense band at 1436 cm^{-1} in the FT-IR spectrum has a maximum contribution from CCH in-plane bending. From the normal mode visualization, it was noted that the bending is of the rocking type. The 1320 cm^{-1} band in the IR spectrum has the character of C−C asymmetric stretching involving carbon (C7) connected to the oxygen and the other two carbon atoms attached (Figure 2). The band observed in the Raman spectrum at 1195 cm^{-1} has a maximum contribution from the CCH bending, which is of the scissoring type. The 998 cm^{-1} band observed in the Raman spectrum is quite intense, which can be assigned to the symmetric ring breathing mode. A corresponding weak band at 999 cm^{-1} was observed in the IR spectrum.

The 1027 cm^{-1} band in the Raman spectrum and corresponding 1033 cm^{-1} band in IR spectrum can be assigned to the asymmetric ring breathing mode. The intense 731 cm^{-1} band observed in the IR spectrum can be assigned to the symmetrical C−H wagging. The 744 cm^{-1} band in the IR spectrum can be correlated with the calculated scaled frequency of 712 cm^{-1}, which has a maximum contribution (32%) from CCC bending and a partial contribution from CS stretching. It is important to note that, although the calculated frequencies are in good agreement with the experimentally observed frequencies, the calculated intensities do not correspond well with experimental intensities. The incorporation of a diffuse function is expected to provide the closer agreement between the calculated and the experimental values.

Triplet State. It is known that TX, upon photoexcitation, leads to various photophysical processes, resulting in the formation of the singlet state, triplet state, exciplex, etc. The 355 nm laser pulse excites TX from the ground electronic state S_0 to the singlet excited state, and then, the intersystem crossing from the singlet electronic states takes place to populate the lowest triplet state.[18] We have recorded the transient absorption spectrum of TX in CCl_4. Figure 3 shows the absorption spectrum of TX in CCl_4 solution in both S_0 and T_1 states. The triplet state has a T−T absorption maximum at ∼648 nm and is expected to be resonance-enhanced at the probe wavelength of 634 nm. Therefore, in the present TR^3 study, we have used a 355 nm laser pulse as a pump to generate the triplet excited state of TX and a 634 nm laser pulse as a probe to record the resonance Raman scattering from the triplet excited state. The 634 nm probe wavelength is within the absorption spectral profile of the triplet excited state, and thus, Raman intensities are resonance-enhanced. The nanosecond TR^3 spectra of the triplet state at various delay times in CCl_4 as a solvent are presented in Figure 4. For better visualization of the decay of the transient species, the solvent bands (doublet) are retained (i.e., without subtraction of the solvent bands from the transient spectra at different delay times). From Figure 4, it is clear that all the bands except the doublet are decaying in intensity with time. We attribute the spectra of the transient state in CCl_4 to the triplet excited state of TX on the basis of following observations: (1) We obtain the transient spectrum only when the probe wavelength is in resonance with the triplet−triplet absorption of TX in CCl4. (2) The decay of the triplet Raman bands with time is consistent with the transient

Table 4. Triplet State Experimental and Calculated Frequencies and Their Tentative Assignments[b]

mode	symmetry	calculated freq (cm^{-1})[a]	experimental freq (cm^{-1})	approx character
ν_{18}	B_2	586	571	sym ring dis
ν_{19}	A_1	644	645	asym ring dis
ν_{34}	A_1	1005	1013	ring breathing
ν_{38}	A_1	1094	1071	ring str + C═O str
ν_3	A_1	1124	1110	ring str + C═O str
ν_{41}	A_1	1139	1130	CH ip bend
ν_{43}	A_1	1212	1165	ring str
ν_{47}	A_1	1338	1377	C═O str
ν_{51}	A	1442	1435	CH ip bend
ν_{53}	A_1	1508	1474	ring str

[a] Calculated with DFT B3LYP/6-31G(d,p); uniform scaling factor = 0.9614. [b] Abbreviations: str, stretching; bend, bending; ip, in-plane; dist, distortion.

absorption studies. (3) No spectral changes other than decay (change in peak position/appearance of new peaks) have been observed with time in the time-resolved resonance Raman spectra. (4) The lowest triplet excited state has been found to be significantly quenched by purging oxygen in the solution.

The mode symmetries, experimental triplet state frequencies, and calculated triplet state frequencies of TX along with tentative band assignments are presented in Table 4. In the TR^3 spectrum of TX in CCl_4, we observe 10 distinct bands. The band at 1013 cm^{-1} is the most intense band in the TR^3 spectrum, which can be tentatively assigned to the symmetric ring breathing mode, which may be correlated with the calculated band at 1005 cm^{-1}. Two bands observed at the 571 and 645 cm^{-1} fit excellently with the calculated values at 586 cm^{-1} and 644 cm^{-1} associated with the ring distortion. On careful normal mode visualization, it has been inferred that the former is due to the symmetric ring distortion (both the rings distort together in the same direction), whereas the later is due to the asymmetric distortion. The band observed at 1130 cm^{-1} in the TR^3 spectrum may be assigned to the CH in-plane bending. This is consistent with the previous transient Raman studies on structurally similar molecules, for example, anthraquinone derivatives.[41,42] This experimentally observed band at 1130 cm^{-1} is consistent with the calculated band at 1139 cm^{-1}. With the help of normal mode analyses, the experimentally observed band at 1165 cm^{-1} is assigned to the ring stretching. The relatively weak bands at 1110 and 1071 cm^{-1} may be assigned to the combined ring and C−O stretch.

In the 1300−1500 cm^{-1} region, two intense bands at 1435 and 1377 cm^{-1} and a weak band at 1474 cm^{-1} have been observed. We assign the 1474 cm^{-1} band as C═C stretching, which is supported by the calculated band at 1508 cm^{-1}. Recently, the structure of the triplet state of xanthone, a structurally similar system, has been investigated by the combined UV/IR study, and the 1459 cm^{-1} band has been assigned to the combined C−C stretching and C−H bending in the infrared.[3] On this basis, we assign 1435 cm^{-1} to the C−H bending mode. The calculated normal mode frequency at 1442 cm^{-1} has the maximum contribution of the CCH bend and can also be correlated to the experimentally observed band at 1435 cm^{-1}. The 1377 cm^{-1} band can be assigned to the C═O stretching. The considerable frequency shift of the C═O vibration from 1622 cm^{-1} (ground state) to 1377 cm^{-1} (triplet state) is consistent with the increase in the C═O distance from 1.23 to 1.30 Å. Interestingly, in the combined UV/IR study by Bartl.et al,[3] the 1293 cm^{-1} band in the IR has been assigned to the C═O vibration of the triplet state of xanthone. This assignment can further be substantiated by the previously reported TR^3 studies on structurally related systems, such as 9,10-anthraquinone and 1-hydroxy anthraquinone, where 1322 and 1329 cm^{-1}, respectively, have been assigned to this mode.[42,43] The calculated value of 1338 cm^{-1} can be correlated with this band. The C═O frequency has also been observed to be very sensitive to the solvent effect.[44]

In the case of aromatic ketones, the C−O stretching frequency of the T_1 state with $\pi-\pi^*$ character lies in the double-bond region, unlike in case of the $n-\pi^*$ T_1 state, which lies in the single-bond region.[45] In the present study, the C−O stretching frequency is distributed among various modes (Table 4) and all the modes with C−O stretching vibration fall in the single-bond region. On this basis, one can assign that the T_1 state of TX in CCl_4 has $n-\pi^*$ character.

SUMMARY

We have presented the vibrational spectroscopic study of TX in S_0 and T_1 states. The ground state has been studied using both Raman and IR techniques, whereas TR^3 spectroscopy has been employed to study the triplet state. The observed bands have been assigned to both the ground as well as the lowest triplet state. From the fact that some of the A2 modes are active in the IR spectrum, it can be concluded that the structure of TX in the ground state is nonplanar. In the triplet excited state, the C═O bond of TX acquires a partial single-bond character that is characteristic of an $n\pi^*$ type excited electronic state of a carbonyl compound.

Electronic excitation distorts the molecule, enabling the increased electron delocalization in the central ring, keeping the ground-state symmetry intact. The largest structural reorganization is observed in the central ring, consisting of an oxygen atom. Normal mode analyses show that the normal mode composition is significantly influenced by the electronic excitation. The C═C stretching and C═O stretching modes are coupled to a greater extent in the triplet state as compared with the ground state. In the ground state, the two high-frequency modes can be assigned almost exclusively to the C═O stretching and C═C stretching, whereas in the transient states, both of these coordinates have comparable contributions to the two totally symmetric modes.

ASSOCIATED CONTENT

Supporting Information. A table of calculated frequencies for TX and its isotopomers in the ground state. This material is available free of charge via the Internet at http://pubs.acs.org.

AUTHOR INFORMATION

Corresponding Author

*Fax: 91-80-23601552. Tel: 91 80-2293 2595. E-mail: umapathy@ipc.iisc.ernet.in.

ACKNOWLEDGMENT

S.U. acknowledges the J.C. Bose fellowship from the Department of Science and Technology. We thank DRDO and CSIR, New Delhi, India, for financial support and the Supercomputer Education and Research Centre of the Indian Institute of Science

for providing the computing facilities necessary to carry out the present work.

REFERENCES

(1) Satzger, H.; Schmidt, B.; Root, C.; Zinth, W.; Fierz, B.; Krieger, F.; Kiefhaber, T.; Gilch, P. *J. Phys. Chem. A* **2004**, *108*, 10072.
(2) Cosa, G.; Lukeman, M.; Scaiano, J. C. *Acc. Chem. Res.* **2009**, *42*, 599.
(3) Kristina, B.; Andreas, F.; Markus, G. *ChemPhysChem* **2009**, *10*, 1882.
(4) Mohapatra, H.; Umapathy, S. *J. Phys. Chem. A* **2009**, *113*, 6904.
(5) Das, D.; Nath, D. N. *J. Phys. Chem. A* **2008**, *112*, 11619.
(6) Shen, L.; Ji, H.-F. *Int. J. Mol. Sci.* **2009**, *10*, 4284.
(7) Balakrishnan, G.; Sahoo, S. K.; Chowdhury, B. K.; Umapathy, S. *Faraday Discuss.* **2010**, *145*, 443.
(8) Corbett, T. H.; Panchapor, C.; Polin, L.; Lowichik, N.; Pugh, S.; White, K.; Kushner, J.; Meyer, J.; Czarnecki, J.; Chinnukroh, S.; Edelstein, M.; LoRusso, P.; Heilbrun, L.; Horwitz, J. P.; Grieshaber, C.; Perni, R.; Wentland, M.; Coughlin, S.; Elenbaas, S.; Philion, R.; Rake, J. *Invest. New Drugs* **1999**, *17*, 17.
(9) Marasanapalle, V.; Li, X.; Polin, L.; Jasti, B. *Invest. New Drugs* **2006**, *24*, 111.
(10) LoRusso, P. M.; Foster, B. J.; Wozniak, A.; Heilbrun, L. K.; McCormick, J. I.; Ruble, P. E.; Graham, M. A.; Purvis, J.; Rake, J.; Drozd, M.; Lockwood, G. F.; Corbett, T. H. *Clin. Cancer Res.* **2000**, *6*, 3088.
(11) Izbicka, E.; Lawrence, R.; Davidson, K.; Rake, J. B.; Von Hoff, D. D. *Invest. New Drugs* **1998**, *16*, 221.
(12) Yates, S. F.; Schuster, G. B. *J. Org. Chem.* **1984**, *49*, 3349.
(13) Anderson, D. G.; Stephen Davidson, R.; Elvery, J. J. *Polymer* **1996**, *37*, 2477.
(14) Zhu, H.; Wang, W.; Yao, S. *Invest. New Drugs* **2006**, *24*, 465.
(15) Dalton, J. C.; Montgomery, F. C. *J. Am. Chem. Soc.* **1974**, *96*, 6230.
(16) Abdullah, K. A.; Kemp, T. J. *J. Photochem.* **1986**, *32*, 49.
(17) Morlet-Savary, F.; Ley, C.; Jacques, P.; Wieder, F.; Fouassier, J. P. *J. Photochem. Photobiol., A* **1999**, *126*, 7.
(18) Ley, C.; Morlet-Savary, F.; Jacques, P.; Fouassier, J. P. *Chem. Phys.* **2000**, *255*, 335.
(19) Ferreira, G. C.; Schmitt, C. C.; Neumann, M. G. *J. Braz. Chem. Soc.* **2006**, *17*, 905.
(20) Krystkowiak, E.; Maciejewski, A.; Kubicki, J. *ChemPhysChem* **2006**, *7*, 597.
(21) Herkstroeter, W. G.; Lamola, A. A.; Hammond, G. S. *J. Am. Chem. Soc.* **1964**, *86*, 4537.
(22) Yip, R. W.; Szabo, A. G.; Tolg, P. K. *J. Am. Chem. Soc.* **1973**, *95*, 4471.
(23) Angulo, G.; Grilj, J.; Vauthey, E.; Serrano-Andres, L.; Rubio-Pons, O.; Jacques, P. *ChemPhysChem* **2010**, *11*, 480.
(24) M.A., E.-S.; Terner, J.; Campion, A. *Proc. Natl. Acad. Sci. U.S.A.* **1977**, *74*, 5212.
(25) Balakrishnan, G.; Mohandas, P.; Umapathy, S. *J. Phys. Chem.* **1996**, *100*, 16472.
(26) Balakrishnan, G.; Umapathy, S. *J. Chem. Soc., Faraday Trans.* **1997**, *93*, 4125.
(27) Balakrishnan, G.; Sahoo, S. K.; Chowdhury, B. K.; Umapathy, S. *Faraday Discuss.* **2010**, *145*, 443.
(28) Du, Y.; Ma, C.; Kwok, W. M.; Xue, J.; Phillips, D. L. *J. Org. Chem.* **2007**, *72*, 7148.
(29) Frisch, M. J.; Trucks, G. W.; Schlegel, H. B.; Scuseria, G. E.; Robb, M. A.; Cheeseman, J. R.; Montgomery, J. A.; Vreven, T.; Kudin, K. N.; Burant, J. C.; Millam, J. M.; Iyengar, S. S.; Tomasi, J.; Barone, V.; Mennucci, B.; Cossi, M.; Scalmani, G.; Rega, N.; Petersson, G. A.; Nakatsuji, H.; Hada, M.; Ehara, M.; Toyota, K.; Fukuda, R.; Hasegawa, J.; Ishida, M.; Nakajima, T.; Honda, Y.; Kitao, O.; Nakai, H.; Klene, M.; Li, X.; Knox, J. E.; Hratchian, H. P.; Cross, J. B.; Bakken, V.; Adamo, C.; Jaramillo, J.; Gomperts, R.; Stratmann, R. E.; Yazyev, O.; Austin, A. J.; Cammi, R.; Pomelli, C.; Ochterski, J. W.; Ayala, P. Y.; Morokuma, K.; Voth, G. A.; Salvador, P.; Dannenberg, J. J.; Zakrzewski, V. G.; Dapprich, S.; Daniels, A. D.; Strain, M. C.; Farkas, O.; Malick, D. K.; Rabuck, A. D.; Raghavachari, K.; Foresman, J. B.; Ortiz, J. V.; Cui, Q.; Baboul, A. G.; Clifford, S.; Cioslowski, J.; Stefanov, B. B.; Liu, G.; Liashenko, A.; Piskorz, P.; Komaromi, I.; Martin, R. L.; Fox, D. J.; Keith, T.; Laham, A.; Peng, C. Y.; Nanayakkara, A.; Challacombe, M.; Gill, P. M. W.; Johnson, B.; Chen, W.; Wong, M. W.; Gonzalez, C.; Pople, J. A. *Gaussian 03*, revision C.02; Gaussian Inc.: Wallingford, CT, 2003.
(30) Ohshima, Y.; Fujii, T.; Fujita, T.; Inaba, D.; Baba, M. *J. Phys. Chem. A* **2003**, *107*, 8851.
(31) Mitsui, M.; Ohshima, Y. *J. Phys. Chem. A* **2000**, *104*, 8638.
(32) Riahi, S.; Norouzi, P.; Bayandori Moghaddam, A.; Ganjali, M. R.; Karimipour, G. R.; Sharghi, H. *Chem. Phys.* **2007**, *337*, 33.
(33) Tomasi, J.; Persico, M. *Chem. Rev.* **1994**, *94*, 2027.
(34) Scott, A. P.; Radom, L. *J. Phys. Chem.* **1996**, *100*, 16502.
(35) Jamróz, M. H. *VEDA 4.0 Program: Vibrational Energy Distribution Analysis*; Warsaw, 2004.
(36) Reed, A. E.; Curtiss, L. A.; Weinhold, F. *Chem. Rev.* **1988**, *88*, 899.
(37) Iijima, K.; Oonishi, I.; Fujisawa, S.; Shibata, S. *Bull. Chem. Soc. Jpn.* **1987**, *60*, 3887.
(38) Sabbah, R.; Elwatik, L. *Can. J. Chem.* **1992**, *70*, 24.
(39) Rubio-Pons, O.; Serrano-Andres, L.; Burget, D.; Jacques, P. *J. Photochem. Photobiol., A* **2006**, *179*, 298.
(40) Wiberg, K. B. *Tetrahedron* **1968**, *24*, 1083.
(41) Kim, Y. H.; Yoon, M.; Cho, D. W.; Jeoung, S. C.; Kim, D. *Bull. Korean Chem. Soc.* **1997**, *18*, 803.
(42) Vauthey, E.; Phillips, D.; Parker, A. W. *J. Phys. Chem.* **1992**, *96*, 7356.
(43) Cho, D. W.; Kim, S. H.; Yoon, M.; Jeoung, S. C. *Chem. Phys. Lett.* **2004**, *391*, 314.
(44) Pandey, R.; Umapathy, S. Understanding Solvent Effect on Thioxanthone Using Time Resolved Resonance Raman Spectroscopy. In *XXII International Conference on Raman Spectroscopy*; Champion, P. M., Ziegler, L. D., Eds.; 2010; Vol. *1267*, pp 1223.
(45) Tanaka, S.; Kato, C.; Horie, K.; Hamaguchi, H.-o. *Chem. Phys. Lett.* **2003**, *381*, 385.